Neutron resonance parameters in ^{155}Gd measured with the DANCE γ-ray calorimeter array

B. Baramsai,[1,*] G. E. Mitchell,[1] U. Agvaanluvsan,[2] F. Bečvář,[3] T. A. Bredeweg,[4] A. Chyzh,[1] A. Couture,[4] D. Dashdorj,[2] R. C. Haight,[4] M. Jandel,[4] A. L. Keksis,[4] M. Krtička,[3] J. M. O'Donnell,[4] R. S. Rundberg,[4] J. L. Ullmann,[4] D. J. Vieira,[4] and C. L. Walker[1]

[1]*North Carolina State University, Raleigh, North Carolina 27695, USA and Triangle Universities Nuclear Laboratory, Durham, North Carolina 27708, USA*

[2]*MonAme Scientific Research Center, Ulaanbaatar, Mongolia*

[3]*Charles University in Prague, Faculty of Mathematics and Physics, V Holešovičkách 2, 180 00 Prague 8, Czech Republic*

[4]*Los Alamos National Laboratory, P. O. Box 1663, Los Alamos, New Mexico 87545, USA*

(Received 30 August 2011; published 27 February 2012)

The ^{155}Gd(n,γ) reaction was measured with the DANCE γ-ray calorimeter at the Los Alamos Neutron Science Center. Spins were determined for the s-wave resonances by analysis of the γ-ray multiplicity distributions. The analysis was performed with a pattern recognition method. The resulting level densities for the $J = 1$ and 2 resonances are in qualitative agreement with the expected $2J + 1$ dependence. The average s-wave resonance spacing was determined to be $D_0 = 1.62 \pm 0.15$ eV. Analysis of the neutron resonances with the code SAMMY yielded the s-wave strength function $S_0 = 1.99 \pm 0.28 \times 10^{-4}$ and the average total radiative width $\Gamma_\gamma = 120 \pm 3$ meV.

DOI: 10.1103/PhysRevC.85.024622 PACS number(s): 25.40.Ny, 21.10.Hw, 25.40.Lw, 21.10.Ma

I. INTRODUCTION

The study of neutron resonances—especially to determine nuclear level densities—is crucial for a wide variety of issues in astrophysics (e.g., nucleosynthesis in stellar environments) and nuclear science (e.g., to constrain reaction models). Improved understanding of the neutron capture reaction in particular is very important for the study of reaction networks in astrophysics, stewardship science, and advanced fuel cycle calculations. The ^{155}Gd measurement also is a nearly ideal choice to examine methods to determine the resonance spin by utilizing the high segmentation of the Detector for Advanced Neutron Capture Experiments (DANCE) array. A common problem in neutron resonance spectroscopy is determining the spin for resonances on targets with nonzero spin. The γ-ray multiplicity method is an approach for determining the spin of neutron resonances that uses the spin dependence of the capture γ-ray spectra. The choice of ^{155}Gd in order to test various methods that use the γ-ray multiplicity for spin determination has several advantages: (i) a reasonable number of levels (nearly 100) to ensure sufficient statistics; (ii) this nucleus is near the peak of the s-wave strength function and the minimum of the p-wave strength function, thus removing the likelihood of ambiguity in the parity assignment; and (iii) there are several excellent previous studies of neutron resonances on ^{155}Gd, enabling thorough testing of various analysis methods.

The DANCE array at the neutron spallation source Los Alamos Neutron Science Center (LANSCE) at the Los Alamos National Laboratory is ideal for this approach. The high segmentation of the DANCE (160 crystals) enables the precise determination of the γ-ray multiplicity distribution. In favorable cases, the average multiplicity is sufficient to determine the resonance spin (see, for example, Ref. [1]). For circumstances where the average multiplicity does not provide sufficient information, more detailed analysis of the multiplicity distribution is required. For this purpose we have developed a novel method to obtain the resonance spin using pattern recognition theory and have applied this method to new capture measurements on ^{155}Gd at DANCE. In addition, we were able to determine resonance parameters, especially neutron widths, for all observed resonances below 185 eV.

In Sec. II the experimental apparatus and data processing is described, while Sec. III describes previous methods that were used to determine the resonance spins from DANCE data. Section IV describes the pattern recognition method. The results of the application of this method are presented in Sec. V together with results of the resonance parameter analysis. Section VI provides a brief summary.

II. EXPERIMENT

The neutron capture experiment on ^{155}Gd was carried out by use of the time-of-flight method at the 20.3-m flight path of LANSCE. The gadolinium target was prepared at the Oak Ridge National Laboratory as a self-supporting metal foil with an area $S = 5.064$ cm^2 and areal density $m = 1.008$ mg/cm^2. The ^{155}Gd (natural abundance 14.80%) target is enriched to 91.74%; the major contaminants are ^{154}Gd, ^{156}Gd, ^{157}Gd, and ^{158}Gd with 0.63%, 5.12%, 1.14%, and 0.94%, respectively. Data were accumulated for about 130 h.

A. DANCE detector

The capture γ rays were measured with the DANCE array. DANCE consists of 160 BaF_2 crystals of four different shapes that are arranged in a 4π geometry. A detailed description of the experimental setup can be found elsewhere [2–4]. The advantages of the detector include (i) the fast timing of the

*bbarams@ncsu.edu

scintillators leads to precise determination of the neutron time of flight; (ii) the fast timing also allows good identification of coincident γ rays following neutron capture; (iii) the detected events can be separated by the Q value of the reaction; and (iv) the high segmentation of the detector enables measurement of the γ-ray multiplicity distribution.

As detailed description of the DANCE data acquisition (DAQ) is given in Ref. [5], and here we mention only some basic features of the system. The pulse from the photomultiplier output of a crystal was digitized in Acqiris DC265 digitizers with 8-bit resolution at a sampling rate of 500 MS/s (mega samples per second). Each waveform was processed on-line to extract the essential parameters which were written to a disk file. The off-line analysis software reads this processed data and reconstructs events.

There are different modes of data acquisition at DANCE; we used the double-continuous mode. In this mode, the signal from all detectors is collected in a 500-μs-wide time window. Three different sets of time-of-flight intervals allow the acquisition of data from 1.36 eV to 1 MeV neutron energy.

The primary energy calibration of the detectors was performed by measuring γ rays from the natural radioactive sources ^{22}Na, ^{60}Co, and ^{88}Y. However, small gain shifts were observed in the light output of each crystal during the course of the experiment, presumably due to temperature changes in the scintillators. Since Ba and Ra are chemical homologs, the BaF_2 crystals always contain radioactive isotopes from the radium decay chain, which turned out to be an advantage: the energies of α particles emitted from these radioactive isotopes could be used to update the gain for each crystal and for each run. As described below, the signals from αs and γs can be distinguished.

B. Experimental spectra

A γ ray often does not deposit all of its energy in a single crystal but rather in several neighboring crystals because of Compton scattering and pair production. The group of adjacent crystals that fire in an event forms a *cluster*. The number of clusters created within a single capture event is called the cluster multiplicity. This multiplicity is much closer to the true multiplicity than is the total number of crystals that fire.

Since DANCE is a calorimetric detector, the origin of events can be recognized by their total energy deposited in the BaF_2 crystals. As shown in Fig. 1 the ^{155}Gd capture events lead to the spectrum of total deposited energy (we denote this spectrum as the *sum-energy spectrum*) with a peak situated near the reaction Q value, 8.536 MeV. This peak originates from the deposition of the full energy of all emitted γ rays, while the tail originates from events in which a part of the emitted energy escapes the detector array. A slight shift in energy of the Q-value peak for ^{155}Gd is due to electron conversion. Only the events in the Q-value peak were considered in the present analysis.

C. Background subtraction

There are several types of background in DANCE experiments: constant background due to natural radioactivity

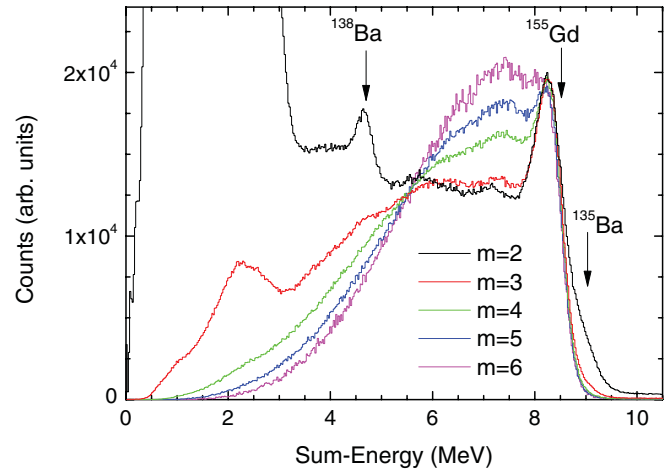

FIG. 1. (Color online) Sum-energy spectra for cluster multiplicities $m = 2$–5 and neutron energy range $E_n = 1.36$–185 eV. The spectrum for each multiplicity was normalized to have the same number of counts in the γ-ray energy range 8.0–8.5 MeV. The arrows indicate the Q value of radiative capture on ^{155}Gd and Ba isotopes: ^{135}Ba with $Q = 9.108$ MeV (natural abundance 6.6%) and ^{138}Ba with $Q = 4.723$ MeV (natural abundance 71.7%). Note that the peak for ^{155}Gd is not at the Q value but is shifted to a lower value due to energy emitted in undetected conversion electrons.

of the BaF_2 scintillators, ambient time-of-flight dependent background, and background from neutrons scattered from the sample.

The constant background from α particles is easily suppressed based on waveform analysis of the signals from the BaF_2 crystals [5]. The scintillation light from the BaF_2 crystals has a fast component (220-nm wavelength, 0.6-ns decay time constant) and a slow component (310-nm wavelength, 600-ns decay time constant). The intensity ratio between the fast and slow components is different for γs and αs, which allows particle identification if both the signal components are measured.

The crystals also contain β activity that arises from the Ra decay chain, such as ^{214}Bi and ^{210}Bi. The energy released in a β decay is at maximum about 2.5 MeV, which makes these decays contribute only to sum energies which are significantly lower than the Q value of the ^{155}Gd(n,γ) reaction (see multiplicities $M = 2$ and 3 in Fig. 1). This means that we can easily eliminate the background from β decay if we use only events around the Q value of the reaction of interest. In the same way, using the Q-value cut, we can eliminate background due to γ rays in the beam. These γ rays are mainly originate from the neutron production area and have energies below 3 MeV [3].

The remaining, target-related background has two components. One comes from neutron capture on target impurities. The Q value for radiative capture in all even Gd targets are below 6.5 MeV. Thus, the contribution from these captures can again be easily avoided by considering only events with sufficiently high detected sum energy—above about 7 MeV. On the other hand, subtracting capture events on ^{157}Gd is more difficult. The Q-value cut is only partly effective since the Q value for the capture on this isotope, $Q(^{157}\text{Gd}) = 7.94$ MeV, is close to the Q value for the capture on

^{155}Gd [$Q(^{155}\text{Gd}) = 8.54$ MeV]. In principle, to remove this background, one can use a much narrower Q-value gate, but this strongly reduces the counting statistics. Fortunately, this background is very small, due to the small amount of ^{157}Gd in the target. As a consequence, even the strongest resonances of this contaminant are seen in our time-of-flight spectra as extremely weak.

The second component of the target related background is due to the capture of neutrons scattered from the target nuclei by Ba isotopes in the detector crystals. In order to reduce this background a ^{6}LiH shell of 6-cm thickness surrounds the target. Despite the absorbing effects of the ^{6}LiH shell some neutrons scattered by the target reach the detector and are captured by the barium in the BaF_2 crystals, producing γ cascades.

The capture γ rays from the Gd target, located at the center of the crystals, are emitted into a 4π solid angle and typically create several clusters. On the other hand, the capture events of the scattered neutrons in the Ba isotopes take place in one of the crystals and usually create only a few clusters. Therefore, the low cluster multiplicity spectra have a high background from the capture of scattered neutrons, while no detectable background is seen at multiplicities $m > 3$. This effect is seen in Fig. 1 where for multiplicities $m = 4$ and 5 the ratio of counts near the energy equal to the ^{135}Ba Q value (9.1 MeV) to the counts at the ^{155}Gd Q value is very small.

The contribution of neutron capture in Ba isotopes can be subtracted using auxiliary measurements with ^{208}Pb. This isotope has a very small capture cross section and an almost constant scattering cross section over a wide neutron energy range. It was found that the spectrum from Ba captures is constant over a wide range of neutron energies.

For a fixed value t of the time of flight, the sum-energy spectra for individual multiplicities M which were obtained from the ^{208}Pb measurement are, except for *a single normalization factor*, identical to the analogous spectra belonging to parasitic γ rays initiated by neutron scattering off ^{155}Gd nuclei and subsequent capture in BaF_2 crystals.

The events at the region above the ^{155}Gd$(n,\gamma)^{156}$Gd reaction Q value in the sum-energy spectrum correspond to the scattered neutrons captured on ^{137}Ba ($Q = 8.612$ MeV) and ^{135}Ba ($Q = 9.108$ MeV) isotopes in the BaF_2 crystals (see Fig. 1). The sum-energy spectra measured with ^{208}Pb and ^{155}Gd targets, thus, could be normalized to the number of events in this region 9.0–9.6 MeV [6]. As can be seen from Fig. 1, the subtracted contribution of γ rays from neutron capture on Ba isotopes is very small, especially for $M \geqslant 3$.

D. Flux measurement

The neutron flux is measured with two different detectors. One of them is a proportional counter filled with BF_3 + Ar gas. This neutron monitor was positioned at 22.76 m from the moderator; the charged particles from the ^{10}B$(n,\alpha)^{7}$Li reaction were measured.

The other detection system consists of ^{6}LiF connected with an n-type surface barrier Si detector. The ^{6}LiF target (thickness 2 μm and size 3×4 cm^2) was deposited on an 8-μm-thick kapton foil and positioned in the center of the beam pipe at a 45° angle approximately 22.59 m from the neutron moderator. The Si detector was located perpendicular to the beam at a distance of 3 cm from the ^{6}Li foil. The tritons and α particles produced in the ^{6}Li$(n,t)^{4}$He reaction were measured.

The neutron beam diverges with increasing distance from the last collimator in the flight path upstream of the DANCE target position. The neutron fluxes measured in the BF_3 and ^{6}Li-Si monitors are, therefore, not the same as the neutron flux at the target position in the center of DANCE. This fact was confirmed with the image plate measurements taken at the beam entry and beam exit of the DANCE array and at the neutron monitor position. The beam spot at the BF_3 monitor has a diameter of ~2.5 cm, whereas the beam spot at the entry to the DANCE ball is approximately 1 cm in diameter.

The method used for flux determination (normalization) at the target position was very similar to that described in Ref. [6]. The 4.9-eV gold resonance cross section was taken as standard and the flux normalization coefficient is determined by the cross section analysis of this resonance. The only difference with respect to Ref. [6] was that the Au target had the same diameter as the Gd target.

E. Estimate of γ efficiency

For determination of resonance parameters it is also important to know the detector response for γ rays with different energies and multiplicities. The efficiency for detecting a single γ ray with the DANCE array was determined by comparing the GEANT4 simulations with experimental data from the calibration sources ^{60}Co, ^{88}Y, and ^{22}Na. Simulations predict that the efficiency for detecting a single emitted γ depends only slightly on γ-ray energy and is at least 85% [4].

The ^{156}Gd compound nucleus usually emits two or more γ rays. The decay pattern was simulated with the Monte Carlo code DICEBOX [7] using realistic models of photon strength functions (PSFs) and level density (LD). The simulated cascades were then processed with the GEANT4 simulations to estimate the total efficiency for detecting a cascade in the selected multiplicity and Q-value range.

Simulations showed that the fraction of detected cascades in the multiplicity window (m = 2–6) and Q-value range (7.0–8.6 MeV) used in the analysis is rather insensitive to the spin of the resonance and to the exact models of PSFs and LD used in the simulations. The fraction reaches a value of about 30.5% of all cascades. The simulated relative difference in efficiency between resonances with different spins and with different (realistic) models of PSFs and LD used in the simulations is at a maximum about 0.5%. The spin independence and the absolute value of the efficiency that were obtained from simulations, seems to be in a very good agreement with the experimental data from strong resonances. In these resonances, the background is very small in general, not only in the Q-value peak, which allows the extraction of the capture yield from all detected events.

III. SPIN DETERMINATION: PREVIOUS METHODS

A neutron captured by the target nucleus forms a compound nucleus at energy $S_n + E_n$ where S_n is the neutron separation

energy. The ground-state spin and parity of the target ^{155}Gd is $3/2^-$. Capturing an s-wave neutron thus leads to $J^\pi = 1^-$ and 2^- resonances in the compound nucleus ^{156}Gd. The electromagnetic decay from these resonances is mainly dipole ($E1$ and $M1$), with a small $E2$ contribution. The ground state of the compound nucleus is usually reached after a few successive γ decays. Different multiplicity distributions can be expected from decay of resonances with different spins to the 0^+ ground state. However, due to expected Porter-Thomas (PT) fluctuations, the multiplicity distributions from different resonances with the same spin will not be exactly the same. If the differences between resonances with the same spin are smaller than the differences between resonances with different spins, then the detected multiplicity distribution can be used to assign a spin to individual resonances.

The capture events detected by the DANCE array can be sorted by their experimental cluster multiplicity m. We shall consider only multiplicities $m = 2$–6 in the rest of this paper. The multiplicity $m = 1$ is excluded as it is highly contaminated with background, especially at weak resonances. In fact, the multiplicity distributions of several very strong resonances indicate that the contribution of multiplicity $m = 1$ events belonging to ^{155}Gd is very small—less than about 4% for both spins. Therefore, the exclusion of $m = 1$ events does not influence the sensitivity of our analysis described below. The contribution to $m \geqslant 7$ is negligible in the experimental data.

In recent years, various implementations of the γ-ray multiplicity method were introduced to assign the spins of neutron resonances measured with the DANCE detector.

A. Average multiplicity

We define the average detected multiplicity $\langle M(E_\lambda)\rangle$ for resonance λ at energy E_λ as the average number of clusters fired in the decay

$$\langle M(E_\lambda)\rangle = \frac{\sum_{m=m_{\min}}^{m_{\max}} m Y_m(E_\lambda)}{\sum_{m=m_{\min}}^{m_{\max}} Y_m(E_\lambda)}, \qquad (1)$$

where $Y_m(E_\lambda)$ is the energy-dependent experimental yield for cluster multiplicity m. In practice, the yields were obtained from summing events over the energy range of the entire resonance. It was shown earlier that in some isotopes the $\langle M(E_\lambda)\rangle$ separate nicely into two groups, see, e.g., the s-wave resonances in ^{95}Mo [1].

As evident from Fig. 2, this is only partially true here. This fact is the consequence of the small difference between the average detected multiplicities for the two resonance spins in ^{155}Gd. The problem becomes more severe with increasing neutron energy—the decrease of the neutron flux with energy leads to larger experimental errors. The average multiplicity method, thus, is not sufficient to determine the ^{155}Gd resonance spins. In addition, this method can be used only for well-isolated resonances. For determination of the spins of closely spaced resonances we need different approaches. They are described below.

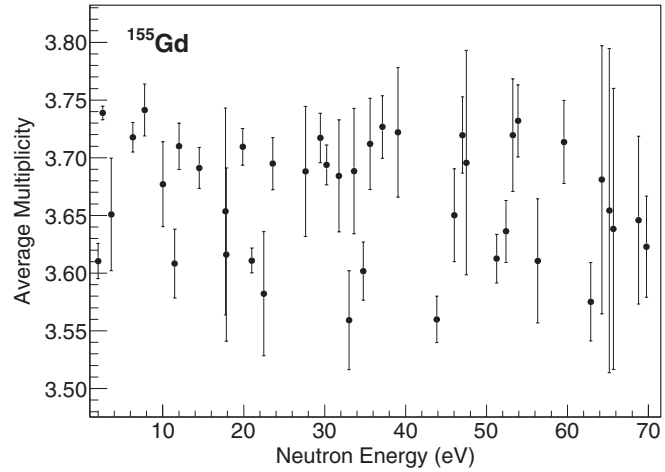

FIG. 2. Average multiplicity of the ^{155}Gd s-wave resonances for neutron energies $E_n = 2$–70 eV. For the resonances at higher neutron energy, errors are usually large due to smaller experimental statistics.

B. Oak Ridge method

Several years ago, Koehler *et al.* [8] introduced a novel version of the γ-ray multiplicity method. They introduced the functions $Z^{(J)}(E)$, where

$$Z^{(1)}(E) = \sum_{m=a}^{b} Y_m^{(1)}(E) - N_{(1)} \sum_{m=c}^{d} Y_m^{(1)}(E) = 0, \qquad (2)$$

$$Z^{(2)}(E) = \sum_{m=a}^{b} Y_m^{(2)}(E) - N_{(2)} \sum_{m=c}^{d} Y_m^{(2)}(E) = 0, \qquad (3)$$

where a, b, c, and d are multiplicities which follow the condition $a \leqslant b < c \leqslant d$, $N_{(J)}$ is a normalization constant, and $Y_m^{(J)}(E)$ is the yield for a resonance with spin J. We have found that the choice 2, 3, 4, and 6 for a, b, c, and d, respectively, gives the best sensitivity of $Z^{(J)}$ to J for our data on ^{155}Gd.

Using isolated resonances for which the spin J is known, the constants $N_{(J)}$ are adjusted so the residual yields of the resonances $Z^{(J)}(E)$ are zero for resonances with spin J. With the assumption that the multiplicity distribution is the same for resonances with the same spin, applying Eq. (2) or Eq. (3) to an arbitrary resonance gives zero or nonzero residuals, depending on the spin of the resonance. Thus, the equations act as spin filters.

As an example, Fig. 3 shows the results of this method in the neutron energy region between 32 and 48 eV. One can easily assign the spins of the strong resonances by examination of the residual yield plot shown in Fig. 3 and even for many of the resonances of average size. However, due to PT fluctuations and experimental errors, one expects some deviation from the assumed ideal behavior. The multiplicity distributions are not exactly the same for all of the resonances with the same spin. This makes spin assignment very uncertain for weak resonances.

In addition, for some resonances both equations yield nonzero residuals–the two spin groups seem to overlap. This effect may be due to spin doublets, but it can also be noise due

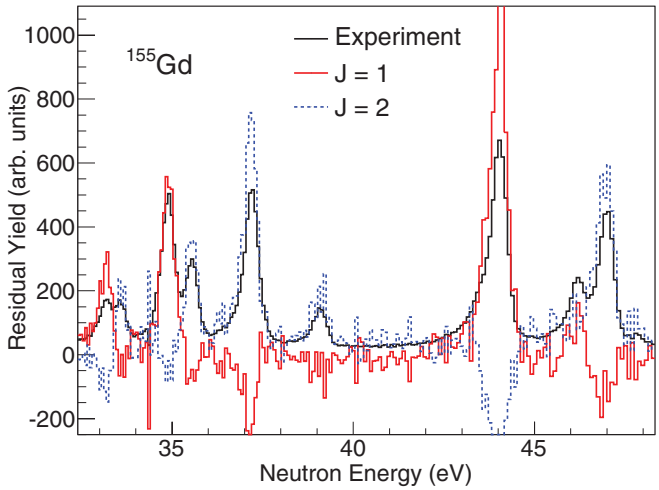

FIG. 3. (Color online) Spin determination of resonances in ^{156}Gd using the Oak Ridge method for $E_n = 32$–48 eV. Nonzero yields of the red and blue lines indicates 1^- and 2^- resonances, respectively. For details see text.

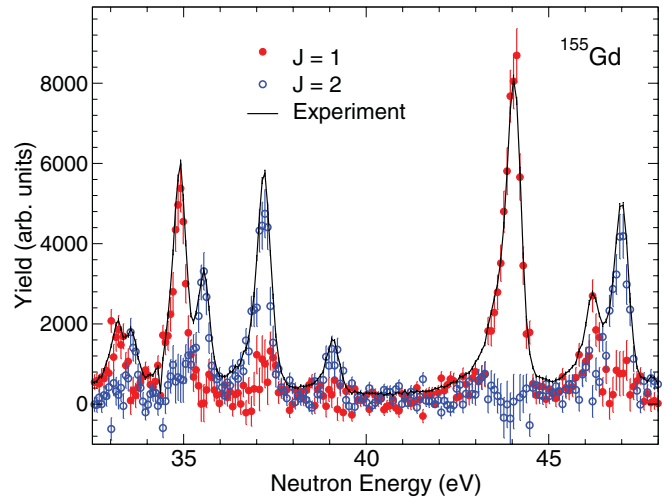

FIG. 4. (Color online) Spin decomposition of the yield with the method of Ref. [9]. The "nonzero residuals" below strong resonances arise due to slightly different multiplicity distributions from different resonances (which is a consequence of the Porter-Thomas fluctuations of the partial radiative widths) and of the experimental errors.

to fluctuations. The combination of weak resonances (poor statistics) and Porter-Thomas fluctuations makes it difficult to assign spins for these resonances.

C. Updated Oak Ridge method

An improvement of the Oak Ridge method was suggested recently [9]. In this approach the fact was used that the experimental yields are a multidimensional vector. If only s-wave neutron capture plays a role, then resonances of two different spins ($J = 1$ and 2 in our case) and one parity are populated.

The normalized yield $y_m(E)$, defined as $y_m(E) = Y_m(E)/\sum_{m=m_{\min}}^{m_{\max}} Y_m$, can then be decomposed as

$$\begin{bmatrix} y_{m_{\min}}(E) \\ y_{m_{\min}+1}(E) \\ \dots \\ y_{m_{\max}}(E) \end{bmatrix} = \begin{bmatrix} \omega_{m_{\min}}^{(1)} & \omega_{m_{\min}}^{(2)} \\ \omega_{m_{\min}+1}^{(1)} & \omega_{m_{\min}+1}^{(2)} \\ \dots & \dots \\ \omega_{m_{\max}}^{(1)} & \omega_{m_{\max}}^{(2)} \end{bmatrix} \begin{bmatrix} \alpha_{(1)}(E) \\ \alpha_{(2)}(E) \end{bmatrix}, \quad (4)$$

where the $\omega_m^{(J)}$ are multiplicity distributions of resonances with spin J and $\alpha_{(J)}(E)$ are the weights for the contributions of spin J at neutron energy E. (In practice one can use Y_m instead of y_m; then $\alpha_{(J)}(E)$ does not correspond to weights but directly to the yield for each spin.) The multiplicity distributions $\omega_m^{(J)}$ were taken from well-isolated resonances of the two possible spins. Two methods for solving Eqs. (4) were suggested in Ref. [9]. The simplest one, which can be used in the case of sufficient statistics, was the least-squares fit method, which minimizes the sum

$$S^2 = \sum_{m=m_{\min}}^{m_{\max}} \frac{1}{\sigma_m^2} \left[y_m(E) - \omega_m^{(1)} \alpha_{(1)}(E) - \omega_m^{(2)} \alpha_{(2)}(E) \right]^2, \quad (5)$$

with respect to $\alpha_{(J)}$. Here σ_m^2 is the experimental error in the value y_m. The results obtained with this method are illustrated in Fig. 4. A different method was developed to solve Eq. (4) which is described in detail in Ref. [9]. This method is especially well suited for weak resonances. Although this approach works very well, especially for doublets, it does not easily provide a quantitative determination of the confidence in the correctness of a given spin assignment.

IV. SPIN DETERMINATION: PATTERN RECOGNITION METHOD

Pattern recognition is a statistical method used to classify data into categories or classes based either on *a priori* knowledge or on statistical information extracted from the patterns [10]. In our problem, the experimental data from each resonance corresponds to a point in "multiplicity space." The points are expected to create clusters in this space depending on the spin and parity of the resonances. Thus, it may be considered as a problem of estimating probability density functions (PDFs) in a multidimensional space and dividing the space into regions of spin groups.

The main advantages of the method may be outlined as follows:

(i) This method does not choose a single resonance as a prototype for the multiplicity distribution of a given spin group of the resonance. Instead, it estimates the density function using the data from the entire data set. Thus, the method considers the variation of the multiplicity distribution due to PT fluctuations and to experimental errors.

(ii) Based on the estimated PDF, it introduces a discriminant function that minimizes the classification error. The hypothesis testing classifies the experimental data into different spin groups and calculates the probability that the spin assignment is correct.

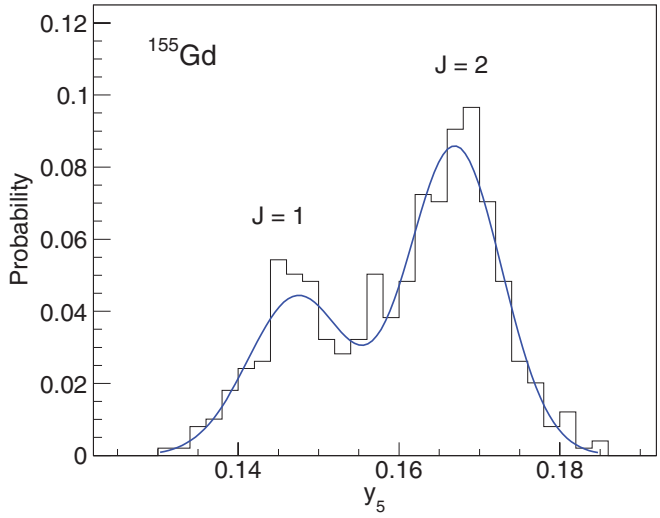

FIG. 5. (Color online) Distribution of the normalized yields, y_5, from resonances of ^{156}Gd. The smooth curve shows fit of the histogram with two Gaussians.

A. Probability density function

In the following we will assume that only s-wave neutron resonances are experimentally observed in ^{155}Gd. The formation of p-wave (or even higher l) resonances is highly unlikely for ^{155}Gd for neutron energies processed here due to the orbital angular momentum potential barrier. In addition, the p-wave neutron strength function is very small in this mass region.

Based on the central limit theorem, we assume that the normalized yields, $y_m(E)$, for a given spin will be normally distributed. Data from well-resolved, strong resonances are used to estimate the parameters of the distribution and set as fixed parameters for all other resonances.

Since we have two spin groups, the PDF is a mixture of two Gaussians for given m. The variances of the Gaussians are the sum of the experimental variance and that which belongs to the PT fluctuations: $\sigma^2 = \sigma^2_{\rm exp} + \sigma^2_{\rm PT}$.

An example of the distribution of normalized yields $y_5(E)$ is shown in Fig. 5. The distributions from the two spin groups are clearly seen here. The two centroids of the distribution correspond to $J^\pi = 1^-$ and $J^\pi = 2^-$ resonances. The difference between the two centroids is about 11%. The distributions of the normalized yields for other multiplicities are similar to those for $m = 5$.

We introduce a vector $\mathbf{y}(E_\lambda) \equiv [y_{m_{\rm min}}(E_\lambda), \ldots, y_{m_{\rm max}}(E_\lambda)]^T$, the components of which represent a probability mass function of the multiplicity for λ-th resonance with energy E_λ. The whole set of vectors $\mathbf{y}(E_\lambda)$ consisting of $\lambda = 1, 2, \ldots, \lambda_N$ will be abbreviated as $\mathcal{Y} \equiv \{\mathbf{y}(E_\lambda)\}$. This data set is assumed to be drawn from a mixture of two multivariate normal distributions in n-dimensional multiplicity space, where $n = m_{\rm max} - m_{\rm min} + 1$.

The joint PDF for this mixed distribution of a random vector $\mathbf{y} \equiv (y_{m_{\rm min}}, \ldots, y_{m_{\rm max}})^T$ can be expressed as

$$g(\mathbf{y}|O) \equiv \beta_{(1)} f_{(1)}\left(\mathbf{y}|\Omega_{(1)}, \Sigma_{(1)}\right) + \beta_{(2)} f_{(2)}(\mathbf{y}|\Omega_{(2)}, \Sigma_{(2)}), \quad (6)$$

where $\Omega_{(k)} = (\omega^{(k)}_{m_{\rm min}}, \ldots, \omega^{(k)}_{m_{\rm max}})^T$ (with $k = 1, 2$) is a vector, the components of which represent expectation values of components of a random vector $\mathbf{y}$ for the case when this vector is governed by the k-th multivariate normal distribution, while $\Sigma_{(k)}$ is the corresponding covariance matrix. The O stands for the set of all parameters, entering the right-hand side of Eq. (6), i.e., $O \equiv (\Omega_{(1)}, \Omega_{(2)}, \Sigma_{(1)}, \Sigma_{(2)}, \beta_{(1)}, \beta_{(2)})$.

The parameters $\beta_{(1)}$ and $\beta_{(2)}$ are the mixing weights that represent the fraction of spin $J = 1$ and $J = 2$ resonances in the sample. The weights can be fixed (using the assumed spin distribution of level density) or fitted to observed distribution. They satisfy the conditions $\beta_{(1)} \geqslant 0$, $\beta_{(2)} \geqslant 0$, and $\beta_{(1)} + \beta_{(2)} = 1$.

The joint PDF of the multivariate normal distribution for spin group k is

$$f_{(k)}(\mathbf{y}|\Omega_{(k)}, \Sigma_{(k)}) = \frac{1}{(2\pi)^{N/2}|\Sigma_{(k)}|^{1/2}} \times \exp\left[-\frac{1}{2}\left(\mathbf{y} - \Omega_{(k)}\right)^{\rm T} \Sigma^{-1}_{(k)}(\mathbf{y} - \Omega_{(k)})\right]. \quad (7)$$

B. Parameter estimation

As stated before, the experimentally observed set of multiplicity distributions $\mathcal{Y}$ is assumed to be drawn at random from the distribution governed by the joint PDF $g[\mathbf{y}(E)|O]$ according to Eq. (6). In principle, the estimates of parameters O can be obtained with the aid of the maximum-likelihood method. However, if the number of fitted parameters is large, the parameters are usually estimated by an iteration method known as the expectation-maximization (EM) algorithm [11].

According to the EM algorithm the parameters obtained in each iteration step are calculated according to the following expressions:

$$\beta_{(k)} = \frac{1}{N}\sum_{\lambda=1}^{N} f_{(k)}\left(\mathbf{y}(E_\lambda)|\Omega^{\rm old}_{(k)}, \Sigma^{\rm old}_{(k)}\right), \quad (8)$$

$$\Omega_{(k)} = \frac{\sum_{\lambda=1}^{N} \mathbf{y}(E_\lambda) f_{(k)}\left(\mathbf{y}(E_\lambda)|\Omega^{\rm old}_{(k)}, \Sigma^{\rm old}_{(k)}\right)}{\sum_{\lambda=1}^{N} \beta^{\rm old}_{(k)} f_{(k)}\left(\mathbf{y}(E_\lambda)|\Omega^{\rm old}_{(k)}, \Sigma^{\rm old}_{(k)}\right)}, \quad (9)$$

$$\Sigma_{(k)} = \frac{\sum_{\lambda=1}^{N} f_{(k)}\left(\mathbf{y}(E_\lambda)|\Omega^{\rm old}_{(k)}, \Sigma^{\rm old}_{(k)}\right)\left(\mathbf{y}(E_\lambda) - \Omega^{\rm old}_{(k)}\right)\left(\mathbf{y}(E_\lambda) - \Omega^{\rm old}_{(k)}\right)^T}{\sum_{\lambda=1}^{N} \beta^{\rm old}_{(k)} f_{(k)}\left(\mathbf{y}(E_\lambda)|\Omega^{\rm old}_{(k)}, \Sigma^{\rm old}_{(k)}\right)}, \quad (10)$$

where the superscript "old" represents the values from previous iteration.

The iterations continue until a steady state is reached, in our case when the change of the parameter values sought is less than 1%. The covariance matrix was set as a diagonal matrix in the first step of the iteration. The initial values of the mean vectors $\mathbf{\Omega}_{(1)}$ and $\mathbf{\Omega}_{(2)}$ were calculated from the multiplicity distribution of strong resonances and the initial value of the $\beta_{(k)}$ were set as equal to 0.5 for both spins.

C. Bayes classifier

The purpose of the analysis is to determine to which class or spin group a given resonance, say, at energy E_λ, belongs. In order to accomplish this purpose, we use the "Bayes decision rule" [11], simply based on Bayes *posterior* probabilities

$$p_1[\mathbf{y}(E_\lambda)] \underset{J_2}{\overset{J_1}{\gtrless}} p_2[\mathbf{y}(E_\lambda)], \tag{11}$$

where

$$p_k[\mathbf{y}(E_\lambda)] = \frac{\beta_{(k)} f_{(k)}\left[y(E)|\Omega_{(k)}, \Sigma_{(k)}\right]}{g(\mathbf{y}\,(E_\lambda)|O)}, \tag{12}$$

where $\beta_{(k)}$ are *prior* probabilities.

To illustrate result of the spin classification based on the use of Bayes decision rule, Fig. 6 shows a two-dimensional scatter plot of $y_3(E_\lambda)$ versus $y_5(E_\lambda)$ for all resonances λ included in our analysis. The spin determination in the figure was based on the use of the whole multiplicity range $m = 2$–6.

As we see from the scatter plot, the probability is a measure where the point lies in the distribution plot. In the case of doublets, where the counts, $\mathcal{Y}$, contain contribution from both $J = 1$ and $J = 2$ resonances, the multiplicity distribution gated on doublet energy region will follow neither $J = 1$ distribution nor $J = 2$ distribution but a mixture of the two distributions. So the point from this energy region will lie in an intermediate region (the crosses in Fig. 6).

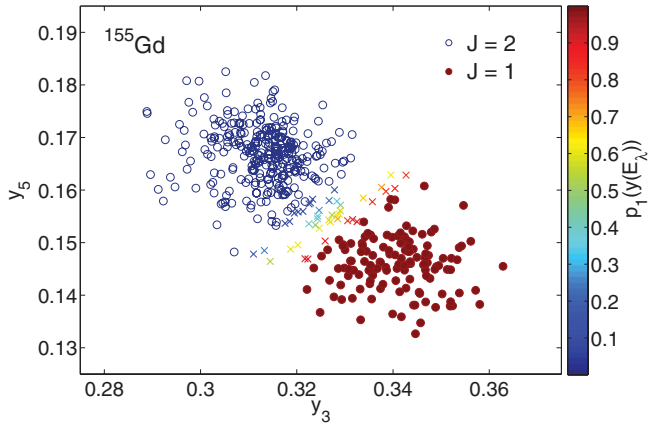

FIG. 6. (Color online) Two-dimensional distribution of normalized yields y_3 and y_5 obtained from resonances in ^{155}Gd. False colors indicate the probability that the spin of the resonance is 1. Crosses correspond to resonances with the probability $p_1[\mathbf{y}(E_\lambda)]$ between 0.1 and 0.9. Full end empty circles then correspond to resonances with $p_1[\mathbf{y}(E_\lambda)] > 0.9$ and < 0.1, respectively.

The method works very well for well-isolated resonances and has the significant advantage of providing a quantitative measure of the reliability of the spin assignment. However, whenever there are contributions from more than one spin (usually doublets), this method is not reliable. In these cases the method described in Ref. [9] is superior for the spin assignment, although a quantitative measure of the confidence in the spin assignment is not explicitly provided.

V. RESULTS FOR ^{155}Gd RESONANCES

A. Spins

Using the methods described above we determined the spins for almost all of the experimentally observed s-wave resonances in ^{155}Gd up to neutron energy $E_n = 185$ eV. Using the pattern recognition method (PRM), we attempted to determine the resonance spins under two different assumptions about weights $\beta_{(J)}$. In one of them, the weights were fixed according to the expected $2J + 1$ dependence of the level density while performing the EC iterations; this corresponds to $\beta_{(1)} = 0.375$ and $\beta_{(2)} = 0.625$. In the other one, $\beta_{(J)}$ was varied in the EM algorithm and the result from the final iteration was $\beta_1 = 0.332$, $\beta_2 = 0.668$. The spin assignments determined by these two approaches were consistent.

As an example of the results obtained, a superimposed plot of the experimental counts and the probabilities for spin $J = 1$ and $J = 2$ obtained with the PRM are shown in Fig. 7 for the resonances in the neutron energy range 32 to 48 eV. The full and open circles above the resonances label spin $J = 1$ and $J = 2$ resonances, respectively. For most cases the probabilities are nearly 100% and the assignments are firm. However, one should be cautious about assignments with lower probabilities. As discussed before, a lower probability may be an indication of spin doublets. For doublets (resonances with different spins), a decision based on the standard PRM is usually not applicable. In these cases, other methods discussed in Sec. III, specifically the Oak Ridge method and its updated version were used for the spin assignment. We found that results from the pattern recognition method and the updated Oak Ridge method were consistent.

Our resonance spin assignments are compared in Table I with values from Refs. [12] and [13]. The probabilities listed in the table are the results based on the use of the EM algorithm. Spins for all resonances with the probabilities higher than 99% are assumed to be firm. On the other hand, all spin assignments with the probabilities lower than 90% are considered to be uncertain. Resonances with probabilities in the 90% to 99% range were examined individually. If the resonance was very weak or poorly resolved, the assignment was considered uncertain. In all other cases cases we give a firm spin assignment. The average multiplicities, $\langle M(E_\lambda)\rangle$, were calculated using Eq. (1).

B. Neutron and total radiative widths

The capture cross section at a particular neutron energy is

$$\sigma_{n,\gamma}(E_n) = \frac{M}{N_A m S \varepsilon_{n,\gamma}(E_n)} \frac{N_{n,\gamma}(E_n)}{\Phi(E_n)}, \tag{13}$$

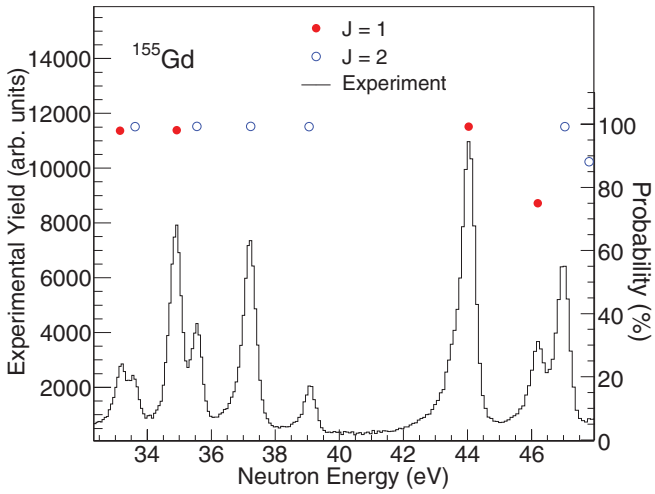

FIG. 7. (Color online) Spin assignments of the neutron resonances in ^{155}Gd based on the pattern recognition method.

where $N_A = 6.022 \times 10^{23}$ mol^{-1} is Avogadro's number, $M = 155$ g/mol is the molar mass of ^{155}Gd, m is the areal density of the target, S is the area of the target, $\varepsilon_{n,\gamma}(E_n)$ is the total efficiency for detecting capture γ rays after applying gates on the event multiplicity and the Q-value cut, $N_{n,\gamma}(E_n)$ is the number of detected capture events, and $\Phi(E_n)$ is the neutron flux. The neutron flux and efficiency were discussed in corresponding subsections of Sec. II.

The measured cross section was used in the determination of neutron, Γ_n, and total radiative widths, Γ_γ. These widths were determined with the multilevel R-matrix Bayesian code SAMMY [14], fitting the capture cross-section data. Doppler broadening, the DANCE timing resolution function, target self-shielding, and multiple scattering corrections were taken into account during the data fitting.

We did not perform transmission measurements. Under these conditions, SAMMY cannot fit both Γ_n and Γ_γ at the same time except in special cases. Both quantities can be obtained simultaneously only for strong low-energy resonances where good energy resolution makes it possible to exploit the detailed resonance shape. In all other cases SAMMY essentially extracts the area A under the resonance which is given by

$$A \sim g\frac{\Gamma_\gamma \Gamma_n}{\Gamma_\gamma + \Gamma_n}, \tag{14}$$

where g is the spin statistical factor.

The radiative width is much greater than the neutron width for almost all fitted resonances in ^{155}Gd. In this case the counts at the resonances are approximately proportional to Γ_n as $A \sim g\Gamma_n$ for $\Gamma_\gamma \gg \Gamma_n$. Therefore, when fitting the resonances that have a dominant radiative channel, SAMMY can produce reliable results only for Γ_n. The results on this quantity are expected to be almost insensitive to the exact value of Γ_γ for the corresponding resonance. Total radiative widths were, thus, fitted with the SAMMY code only for several strong resonances and were fixed for the rest of resonances to the expectation value of $\Gamma_\gamma^{(\mathrm{exp})} = 120(3)$ meV, which was obtained from the fitted resonances. The value of $\Gamma_\gamma^{(\mathrm{exp})}$ is in agreement with RPI measurements [13], $\Gamma_\gamma^{(\mathrm{exp})} = 121(4)$ meV, but is slightly higher than the value given in Ref. [12] of $\Gamma_\gamma^{(\mathrm{exp})} = 110(3)$ meV. Neutron widths obtained in this manner are listed in Table II.

To obtain an estimate of the sensitivity of the extracted value of Γ_n to the value assumed for Γ_γ, we also ran the SAMMY code with two fixed values, $\Gamma_\gamma^{\min}$ and $\Gamma_\gamma^{\max}$, that corresponded to our estimate of the minimum and maximum possible value of the total radiative width.

The statistical model predicts that due to the many possible decay channels the Γ_γ should not vary much for resonances in a given isotope. This quantity is also expected to depend only weakly on the spin of the compound nuclear resonance. Simulations of the γ decay of resonances in ^{155}Gd with the DICEBOX code indicated that the fluctuation in Γ_γ due to PT fluctuations was expected to be about 2 or 3% for resonances with the same spin. The simulations also predicted only a small difference, again about 2 or 3%, between the expectation values of total radiative widths for resonances with different spins.

We decided to set $\Gamma_\gamma^{\min} = 105$ meV and $\Gamma_\gamma^{\max} = 135$ meV. If the statistical model is applicable to γ decay of these neutron resonances, all s-wave resonances in ^{155}Gd should have Γ_γ between $\Gamma_\gamma^{\min}$ and $\Gamma_\gamma^{\max}$. This expectation agrees with experimentally determined values. The differences in Γ_n obtained with the two limiting cases are shown in Fig. 8. The difference $\Delta\Gamma_n$ in the figure is defined as

$$\Delta\Gamma_n(\%) = 100\frac{\Gamma_n\left(\Gamma_\gamma = \Gamma_\gamma^{\min}\right) - \Gamma_n\left(\Gamma_\gamma = \Gamma_\gamma^{\max}\right)}{\Gamma_n(\Gamma_\gamma = \langle\Gamma_\gamma\rangle)}, \tag{15}$$

where $\Gamma_n(\Gamma_\gamma = \bullet)$ stands for neutron width obtained with Γ_γ fixed to $\bullet$, and $\langle\Gamma_\gamma\rangle$ is the expectation value of Γ_γ given in Table I. As can be seen, the uncertainty in the knowledge of exact Γ_γ for a resonance gives only a small (less than 6% for more than 90% of resonances) additional uncertainty to the values of Γ_n. In other words, the area under the resonances is insensitive to the radiative width for the large majority of resonances. However, as expected, some low energy and/or strong resonances are sensitive to the radiative width. For these resonances SAMMY can reliably determine both Γ_n and Γ_γ. SAMMY was used to fit Γ_γ for all resonances for which the difference in neutron width obtained with fixed $\Gamma_\gamma^{\min}$ and $\Gamma_\gamma^{\max}$ was higher than 5%. The uncertainty shown in Fig. 8 was added to errors in Γ_n in Table I for those resonances for which Γ_γ was fixed to 120 meV in the analysis. On the other hand, for resonances for which Γ_γ was determined from theSAMMY fit, the uncertainty shown in Fig. 8 was not included in the error given in Table I. The fit of the measured cross section in the neutron energy range $E_n = 1.4$–185 eV is shown in Fig. 9.

In addition to uncertainties in Γ_n given in Table I and Fig. 8 there are also systematic uncertainties in determination of the cross section via Eq. (13) which then propagate to the uncertainty in Γ_n. Specifically, these uncertainties are in the areal density (m) and area (S) of the target, the neutron flux (Φ), and the detection efficiency $\varepsilon_{n,\gamma}$. The uncertainty in the areal density and the area of the target is very small, about 0.5%. The uncertainty in the flux was determined from the

TABLE I. The resonance parameters for ^{155}Gd isotopes.

Mughabghab [12]				Leinweber*et al.* [13]			This work						
E_n (eV)	$J^{\ddagger}$	$2g\Gamma_n$ (meV)	Γ_γ (meV)	E_n (eV)	$2g\Gamma_n$ (meV)	Γ_γ (meV)	E_n (eV)	$2g\Gamma_n$ (meV)	Γ_γ (meV)	$J^{\ddagger}$	Prob. (%)	$\langle M_J \rangle$	Note
2.008(10)	1	0.278(3)	110(1)	2.012(2)	0.3(1)	128(1)	2.02(1)	0.27(1)	112(2)	1	99.5	3.61(1)	
2.568(13)	2	2.18(2)	111(1)	2.5729(3)	2.138(3)	107(4)	2.575(10)	2.19(2)	107(2)	2	100	3.74(1)	
3.616(6)	–	0.033(2)	130(17)	3.616(3)	0.038(2)	130	3.62(3)	0.031(2)	121(2)	[1]	75.8	3.65(4)	a
6.3(2)	2	2.50(15)	114(7)	6.3057(2)	2.75(1)	109(1)	6.31(1)	2.71(3)	114(3)	2	100	3.72(1)	
7.75(1)	2	1.40(5)	124(4)	7.7477(4)	1.45(1)	109(1)	7.76(1)	1.42(2)	119(4)	2	100	3.74(2)	
10.01(1)	2	0.21(2)	115(20)	9.991(3)	0.25(4)	110(20)	10.02(2)	0.23(1)	120	2	99.9	3.67(3)	
11.53(1)	1	0.45(3)	125(23)	11.508(1)	0.58(8)	120(40)	11.53(3)	0.46(1)	120	1	90.5	3.6(2)	
11.99(1)	2	1.10(5)	112(11)	11.964(8)	1.4(4)	130(20)	11.99(2)	1.32(2)	121(5)	2	99.9	3.71(2)	
14.51(1)	2	2.4(2)	103(10)	14.476(9)	2.57(9)	130(10)	14.50(2)	2.45(4)	126(5)	2	100	3.69(1)	
17.77(2)	2	0.49(3)	120(25)	17.729(5)	0.59(4)	130(40)	17.73(3)	0.31(2)	120	2	99.5	3.65(7)	
–	–	–	–	–	–	–	17.81(3)	0.23(2)	120	[1]	68	3.61(6)	b
19.92(2)	2	5.7(4)	104(16)	19.86(1)	5.63(1)	118(6)	19.91(3)	6.1(10)	120	2	99.9	3.71(1)	
21.03(4)	1	19.5(9)	98(6)	20.97(2)	14.5(2)	140(20)	21.01(2)	14.93(3)	130(4)	1	99.8	3.61(1)	
–	–	–	–	–	–	–	22.45(2)	0.28(5)	126(4)	[1]	92.1	3.57(4)	c
23.67(4)	2	3.9(1)	120(15)	23.6(2)	3.64(8)	140(10)	23.62(3)	3.7(6)	120	2	99.7	3.69(2)	
27.57(5)	2	0.84(2)	125(20)	27.509(2)	0.98(4)	140(20)	27.55(5)	0.83(2)	120	2	100	3.68(5)	
29.58(5)	2	5.4(4)	108(22)	29.5(2)	6.0(1)	113(2)	29.54(6)	6.8(3)	120	2	99.9	3.72(2)	
30.10(6)	2	13(3)	100(11)	30.05(2)	13.9(5)	130(10)	30.10(4)	13.8(2)	124(15)	2	99.8	3.69(1)	
31.72(6)	2	1.40(4)	118(20)	31.66(1)	1.55(7)	140(20)	31.69(6)	1.4(3)	120(8)	2	99.8	3.68(4)	
33.14(7)	–	1.4(3)	110	33.1(2)	1.2(6)	110(30)	33.09(7)	1.51(8)	120	1	98.6	3.55(3)	a
33.51(7)	2	1.2(3)	115(35)	33.4(3)	0.7(3)	120(90)	33.49(8)	1.35(4)	120	2	99.9	3.68(4)	
34.83(7)	1	4.6(3)	152(23)	34.73(2)	5.1(2)	131(4)	34.80(8)	4.7(2)	123(6)	1	98.8	3.6(2)	
35.47(7)	2	2.30(12)	118(23)	35.39(1)	2.71(6)	140(10)	35.43(6)	2.42(7)	128(8)	2	100	3.72(3)	
37.12(8)	2	6.3(2)	101(20)	37.066(3)	6.2(3)	139(6)	37.11(4)	5.9(2)	120	2	100	3.73(2)	
39.00(8)	2	1.3(2)	118(23)	38.93(1)	1.56(7)	130(60)	38.98(6)	1.28(5)	120	2	99.9	3.73(5)	
43.92(10)	1	13(1)	136(9)	43.83(7)	13.5(67)	140(90)	43.89(5)	14.1(11)	120	1	99.9	3.56(2)	
46.1(1)	1	2.8(2)	126(20)	45.98(2)	2.9(1)	128(6)	46.03(4)	2.8(1)	127(8)	[1]	75.6	3.65(3)	
46.87(10)	2	6.7(3)	100(12)	46.79(2)	12.7(4)	140(30)	46.86(6)	6.7(1)	130(10)	2	99.9	3.72(3)	
47.73(11)	1	0.49(4)	110	47.628(6)	0.29(3)	107(10)	47.67(2)	0.33(3)	116(11)	[2]	88.7	3.71(8)	d
51.38(11)	1	14.0(7)	110	51.25(3)	15.2(6)	130(30)	51.34(10)	15.0(7)	120	1	99.6	3.61(2)	
52.13(12)	1	14.6(5)	115(39)	52.01(3)	15.7(8)	140(20)	52.09(8)	16.1(12)	120	1	99.0	3.64(2)	
53.03(8)	1	1.70(6)	110	52.89(2)	1.5(2)	80(30)	53.01(3)	1.7(1)	117(11)	[2]	90.0	3.72(4)	d
53.74(8)	2	9.6(7)	92(20)	53.62(2)	10.9(2)	140(30)	53.68(6)	10.1(3)	117(7)	2	100	3.74(3)	
56.22(8)	1	2.7(2)	120(18)	56.12(1)	3.1(1)	120(40)	56.16(7)	2.6(1)	117(12)	1	97.4	3.62(4)	
59.32(9)	2	8.3(2)	129(19)	59.3(1)	8.6(4)	140(40)	59.35(6)	8.8(3)	120	2	100	3.72(3)	
62.84(9)	1	10.0(4)	90(15)	62.73(2)	10.6(5)	150(30)	62.77(8)	9.9(4)	119(9)	1	99.9	3.58(3)	
64.09(10)	1	0.32(4)	110	64.028(6)	0.61(5)	110(40)	64.23(5)	0.22(1)	120	[2]	98.9	3.71(10)	d
65.2(11)	2	1.0(2)	110	66.4(5)	0.4(4)	120(10)	65.10(6)	0.52(4)	120	[1]	63.9	3.68(11)	d
68.78(11)	[1]	–	–	–	–	–	68.81(6)	0.44(5)	120	[2]	82.5	3.66(6)	d,e
69.4(1)	1	7.9(3)	110	69.4(1)	15(5)	100(100)	69.53(6)	7.9(4)	102(8)	1	99.1	3.61(4)	
77.0(1)	[2]	2.0(1)	110	76.85(1)	3.7(3)	110(60)	76.88(2)	1.9(1)	120	[2]	98.5	3.61(7)	
77.8(1)	[1]	0.90(5)	110	77.63(1)	0.7(1)	110(20)	77.69(2)	0.9(2)	120	[1]	98.9	3.59(9)	
78.8(1)	2	5.3(5)	110	78.75(6)	10.0(12)	110(30)	78.81(7)	5.5(2)	120	2	99.9	3.66(5)	
80.05(12)	[2]	0.39(14)	110	80(3)	0(3)	112(4)	80.17(8)	0.3(3)	120	[1]	84.1	3.5(8)	d
80.9(1)	[2]	1.8(2)	110	80.9(3)	1.08(8)	110(30)	80.77(8)	1.91(8)	120	[2]	99.0	3.66(9)	
84.2(1)	2	6.9(2)	110	83.97(2)	7.7(1)	120(40)	84.01(6)	6.9(3)	120	2	100	3.67(4)	
85.0(1)	2	2.30(12)	110	84.91(1)	1.65(3)	110(40)	84.95(18)	2(1)	120	2	100	3.63(9)	
90.50(13)	[2]	1.60(6)	110	90.51(2)	3.1(2)	110(90)	90.5(4)	0.9(2)	120	[1]	98.6	3.52(10)	d
92.50(15)	–	2.70(29)	110	92.47(2)	2.67(6)	110(20)	92.4(8)	2.7(3)	120	[1]	52.9	3.58(9)	a
92.8(2)	–	3.90(36)	110	92.9(3)	4.35(7)	110(50)	92.9(8)	3.7(3)	120	[2]	87.6	3.57(9)	a
94.1(15)	[1]	0.68(5)	110	93.99(1)	0.8(1)	110(40)	94.2(2)	0.39(6)	120	[1]	76	3.61(19)	
95.7(2)	–	4.80(33)	110	95.7(3)	8.9(4)	110(50)	95.7(2)	4.6(2)	120	2	96.8	3.62(5)	a
96.6(2)	1	4.70(31)	110	96.4(2)	2.8(7)	110(50)	96.4(3)	4.6(4)	120	[1]	88.3	3.58(6)	
98.3(2)	–	13.00(39)	110	98.3(3)	8.8(4)	150(20)	98.3(3)	12.1(5)	120	2	100	3.71(4)	a

TABLE I. (*Continued.*)

Mughabghab				RPI			This work						
E_n (eV)	$J^{\ddagger}$	$2g\Gamma_n$ (meV)	Γ_γ (meV)	E_n (eV)	$2g\Gamma_n$ (meV)	Γ_γ (meV)	E_n (eV)	$2g\Gamma_n$ (meV)	Γ_γ (meV)	$J^{\ddagger}$	Prob. (%)	$\langle M_J \rangle$	Note
100.2(1)	2	1.6(2)	110	99.9(1)	1.9(2)	110(10)	100.3(1)	1.2(1)	120	[2]	88.5	3.6(10)	
101.4(1)	–	3.4(3)	110	101.42(2)	2.6(2)	140(30)	101.4(4)	2.8(2)	120	2	99.6	3.66(8)	a
102.1(1)	–	1.3(2)	110	102.03(3)	1.14(60)	110(50)	102.1(4)	1.4(2)	120	[1]	97.5	3.52(10)	a
104.4(1)	1	6.8(8)	110	104.36(9)	3.7(9)	110(80)	104.5(9)	5.9(4)	120	1	99.9	3.56(5)	
105.9(1)	2	4.6(4)	110	105.8(1)	4.5(8)	140(20)	106.0(4)	4.4(3)	120	2	100	3.63(7)	
107.1(1)	1	7.8(6)	110	107.14(4)	11.2(25)	110(80)	107.1(3)	7.6(5)	120	[1]	85.3	3.59(6)	
109.6(1)	2	3.5(3)	110	109.37(2)	5.5(4)	115(2)	109.6(3)	2.8(0.2)	120	2	99.4	3.62(7)	
112.4(1)	2	11.3(15)	84(10)	112.4(4)	11.4(3)	90(70)	112.4(3)	12.1(6)	120	2	99.7	3.69(5)	
113.8(2)	1	19(3)	67(12)	113.81(5)	25.0(12)	130(20)	113.9(5)	22.0(25)	120	1	99.9	3.59(4)	
116.5(2)	2	13.0(17)	116(94)	116.56(6)	15.7(6)	120(80)	116.6(2)	14.1(19)	120	2	99.8	3.67(5)	
–	–	–	–	–	–	–	116.9(2)	1.5(5)	120	[1]	96.5	3.64(10)	b
118.6(2)	2	2.5(2)	109.8	118.66(2)	3.1(5)	110(50)	118.8(2)	2.6(2)	120	[2]	98.9	3.63(9)	
123.4(2)	2	27.0(43)	159(65)	123.35(5)	30.0(45)	200(100)	123.4(3)	29.2(9)	124(30)	2	100	3.72(3)	
124.4(2)	[2]	8.3(9)	110	124.49(3)	5(12)	120(20)	124.5(2)	7.8(5)	120	[2]	88.1	3.66(7)	
126.0(2)	2	15.4(21)	110	126.11(2)	10.9(3)	110(60)	126.1(4)	16.1(7)	120	2	99.4	3.67(5)	
128.6(2)	[1]	1.40(17)	110	128.53(2)	2.1(3)	110(30)	128.9(2)	0.68(18)	120	[1]	61.3	3.58(11)	
129.8(2)	–	3.20(53)	110	129.82(1)	4.2(4)	110(40)	129.8(2)	3.8(3)	120	2	98.5	3.61(7)	a
130.8(2)	[1]	36.4(57)	110	130.79(1)	16.5(22)	150(30)	130.9(2)	33.2(27)	122(18)	[1]	51.5	3.63(4)	
133.0(2)	–	2.8(4)	110	133.04(1)	4(3)	140(20)	133.1(5)	3.3(3)	120	[2]	99.0	3.61(10)	a
133.8(2)	–	2.9(5)	110	133.95(1)	4.2(3)	110(30)	133.9(2)	2.9(4)	120	[1]	93.0	3.54(16)	a
134.7(2)	–	1.1(2)	110	135.13(2)	2.4(2)	110(60)	134.6(5)	0.9(1)	120	[2]	99.0	3.63(9)	a
137.8(2)	2	16.0(15)	110	137.99(8)	67(22)	120(80)	137.8(9)	8.8(5)	120	2	99.8	3.63(9)	
–	–	–	–	–	–	–	138.0(7)	6.9(5)	120	[1]	99.4	3.54(9)	b
140.4(2)	2	3.10(34)	110	140.55(5)	3.7(2)	130(10)	140.5(8)	2.4(3)	120	[1]	99.0	3.52(14)	d
141.4(2)	–	1.30(21)	110	141.3(1)	2.1(1)	120(10)	141.3(2)	0.7(1)	120	[2]	98.7	3.6(10)	a
145.6(2)	[2]	7.7(7)	110	145.66(1)	8.1(4)	150(20)	145.6(1)	6.8(4)	120	2	100	3.67(6)	
146.9(2)	–	4.7(6)	110	147.02(1)	6.6(3)	130(10)	146.9(5)	5.3(4)	120	[2]	98.9	3.64(7)	a
148.2(2)	[1]	12.0(14)	110	148.4(3)	10.7(11)	110(10)	148.2(2)	12.0(10)	120	[1]	54.7	3.6(6)	
149.6(2)	–	25.0(72)	110	149.53(3)	27.0(15)	110(40)	149.5(6)	23.0(32)	115	[1]	67.5	3.62(4)	a
150.2(2)	–	31(11)	110	150.37(4)	100(37)	110(40)	150.2(8)	32.0(26)	120	2	98.8	3.67(4)	a
152.2(2)	1	6.0(5)	110	152.27(1)	4.6(7)	150(40)	152.2(5)	6.2(5)	120	[1]	98.4	3.54(8)	
154(2)	–	1.4(2)	110	153.8(5)	1.4(3)	160(30)	154.2(3)	0.73(6)	120	[2]	86.6	3.51(11)	a
156.3(2)	1	9.6(8)	110	156.4(1)	37.5(12)	110(80)	156.3(6)	9.2(7)	120	1	99.9	3.55(7)	
160.1(2)	2	12.0(13)	110	160.03(7)	12.9(6)	110(50)	160.1(16)	11.3(8)	120	2	100	3.7(6)	
161.6(2)	2	25.0(32)	110	161.57(8)	27(1)	150(20)	161.6(4)	20.7(7)	120	2	100	3.72(6)	
168.3(2)	2	22.6(24)	110	168.2(9)	23(3)	123(6)	168.3(2)	20.6(12)	120	2	100	3.71(5)	
170.3(2)	–	10.4(15)	110	170.2(1)	10.0(12)	80(30)	170.2(6)	11.8(10)	120	1	98.7	3.66(6)	a
171.4(2)	–	11.5(16)	110	171.6(1)	22.5(12)	110(60)	171.4(3)	10.3(6)	120	2	99.9	3.66(7)	a
173.5(2)	2	41(5)	110	173.5(1)	41.2(25)	110(80)	173.6(6)	41.0(33)	117(12)	2	99.9	3.68(5)	
175.6(2)	[2]	2.60(29)	110	175.46(5)	5.2(7)	110(40)	175.2(2)	1.6(2)	120	[2]	96.7	3.57(11)	
178.0(2)	2	7.3(7)	110	177.99(2)	9.7(15)	130(10)	178.0(12)	6.6(4)	120	2	100	3.72(8)	
180.4(3)	2	11.0(11)	110	180.34(4)	7.3(2)	110(40)	180.3(5)	9.7(6)	120	2	99.7	3.65(8)	
183.3(3)	1	8.0(8)	110	183.2(5)	1.3(2)	110(40)	183.1(3)	11.5(9)	120	1	93.1	3.55(8)	

[‡]The brackets indicate uncertain spin assignment. A criterion used for J assignment from "This work" is mentioned in Sec. VA.

[a]New spin assignment.

[b]Multiplicity distribution suggests new doublet.

[c]There are resonances at about 22.3 eV in ^{154}Gd and ^{158}Gd in Ref. [12] but the our sum-energy spectrum also clearly indicates a resonance in ^{155}Gd.

[d]Spin assignment differs from Ref. [12].

[e]The resonance was not assigned in ENDF/B-VII.0 and JENDL-4.0 but it is in JEFF-3.1 and ROSFOND-2010.

difference in the flux obtained with the two neutron monitors described in Sec. II D; this uncertainty is at a maximum of about 3%. The uncertainty in the efficiency for detection of γ rays in the the range of sum energies and multiplicities employed in the analysis can be estimated from the DICEBOX + GEANT4 simulations mentioned in Sec. II E. We estimate

TABLE II. Average level spacings based on experimental observations. All observed resonances to given neutron energy E_n were considered.

E_n (eV)	$N_{J=1}$	$D_{0,1}$ (eV)	$N_{J=2}$	$D_{0,2}$ (eV)	D_0 (eV)	$D_{0,1}/D_{0,2}$
60	13	4.51(91)	22	2.70(42)	1.69(21)	1.67(42)
100	21	4.72(75)	33	2.96(37)	1.82(18)	1.59(32)
140	30	4.69(62)	47	2.93(31)	1.80(15)	1.60(27)
180	35	4.94(61)	60	2.96(27)	1.85(14)	1.68(26)

this uncertainty to be at a maximum about 3%. The combined systematic uncertainty in Γ_n is, thus, estimated to be smaller than 5%. This uncertainty is not reflected in Table I and Fig. 8.

A comparison of our Γ_n values with those from Mughabghab [12] and Leinweber*et al*. [13] is listed in Table I; the difference in the widths is shown in Fig. 10 in the form of residuals δ

$$\delta = \frac{\Gamma_n^{(\text{our})} - \Gamma_n^{(\text{lit})}}{\sqrt{\text{Var}\left[\Gamma_n^{(\text{our})}\right] + \text{Var}\left[\Gamma_n^{(\text{lit})}\right]}}, \quad (16)$$

where the superscript "lit" stand for values in the literature and Var is the variance of the corresponding values.

The neutron widths obtained from our measurement agree within experimental errors with the previously published Evaluated Nuclear Data File (ENDF) values [12]. There are only two points in Fig. 10 with the difference larger than three standard deviations. We give a comment on both these cases here.

The smaller value of Γ_n from our measurement for the resonance at about 138 eV arises from the fact that we suggest a doublet of resonances here. The sum of neutron widths for the proposed doublet is within uncertainties the same as the value given Ref. [12]. Our Γ_n of 21.0 eV resonance is almost precisely 3/4 of the value given in Ref. [12]. As our value reasonably agrees with the value from Ref. [13], perhaps the value in Ref. [12] corresponds to Γ_n instead of $2g\Gamma_n$. The agreement with the values from Ref. [13] is, in general, not as good.

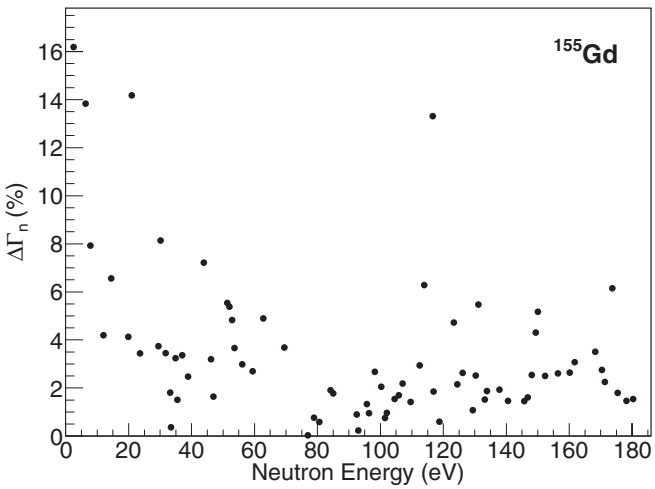

FIG. 8. Sensitivity of Γ_n on adopted value of Γ_γ. Definition of $\Delta\Gamma_n$ is given in Eq. (15).

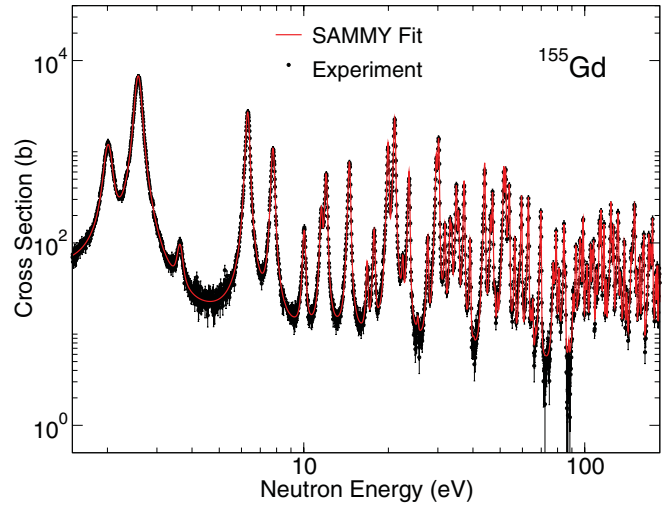

FIG. 9. (Color online) SAMMY fit of experimentally measured cross section in the energy region of our interest.

C. Average resonance parameters

Average resonance parameters of s-wave resonances—specifically, the neutron strength function, S_0, and the average resonance spacing, D_0—can be obtained from information given in Table I.

1. Neutron strength function

The estimate of the neutron strength function can be calculated as

$$S_0 = \frac{1}{\Delta E}\sum_{\Delta E} g_J \Gamma_n \left(\frac{1\text{ eV}}{E}\right)^{1/2} = \frac{1}{\Delta E}\sum_{\Delta E} g_J \Gamma_n^0, \quad (17)$$

where ΔE is the interval of neutron energies which the reduced neutron widths are summed over. Resonances of both spins

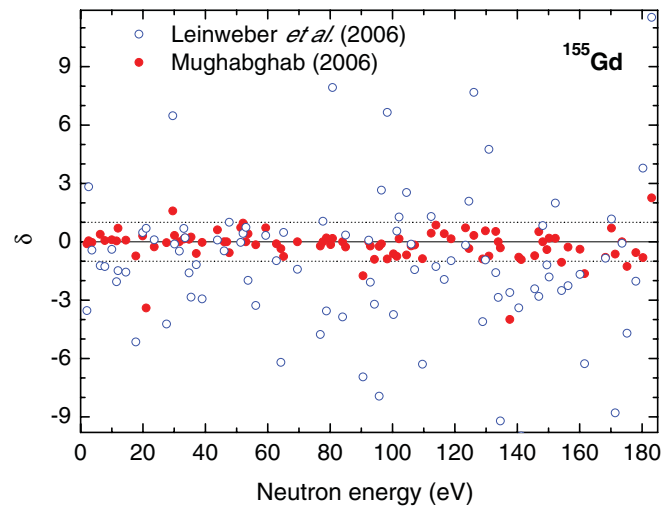

FIG. 10. (Color online) Difference between our neutron widths and values available in the literature, Mughabghab (2006) [12] and Leinweber*et al*. (2006) [13]. The difference is expressed in terms of residuals δ defined in Eq. (16). The agreement within one standard deviation is indicated with dotted lines.

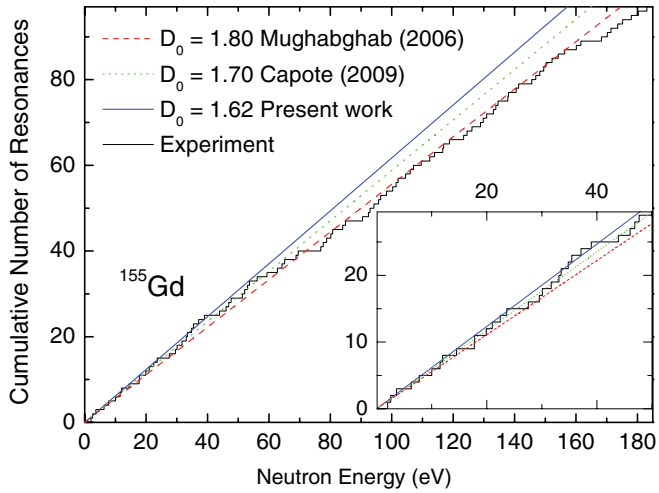

FIG. 11. (Color online) Cumulative number of observed resonances as a function of neutron energy. For comparison, lines corresponding to average spacings from Mughabghab (2006) [12] and Capote *et al.* (2009) [15] are plotted. The inset is a closeup of the plot at low neutron energies.

contribute to $\sum g\Gamma_n^0$. The uncertainty in S_0 is given by the uncertainty in $\sum \Gamma_n^0$, which is obtained from SAMMY fitting, and by the PT fluctuations which the individual Γ_n^0 are expected to follow. The PT fluctuation adds an uncertainty $\sqrt{2/N}S_0$, where N is the number of resonances.

There is almost no chance of observing all of the resonances. Some are very weak due to PT fluctuations. On the other hand, if the experiment has a sufficiently low threshold for observation of resonances (which is the case for the ^{155}Gd(n,γ) experiment), the missing strength is very small. An estimate of the missing strength was obtained using realistic parameters of the neutron strength function, the average resonance spacing (see discussion below), and the threshold for observation of ^{155}Gd resonances. We estimate the fraction of missing strength at a maximum of about 2% below the 185-eV neutron energy. The estimate of S_0 using Eq. (17) is, thus, reasonable, as the missing strength is much smaller than the uncertainty arising from the PT distribution itself as well as from the experimental uncertainty in $\sum \Gamma_n^0$. Our data yield $S_0 = 1.99(28) \times 10^{-4}$, in agreement with the value $S_0 = 2.20(14)$ in Ref. [12]. A possible systematic error of about 5% in S_0 due to Γ_n, discussed in Sec. V B, is not included here.

2. *Resonance spacing*

It should be stressed that the sensitivity for observation of neutron resonances in our experiment is similar to previous ones—only four new resonances were observed. As a consequence, our average spacing should be similar to values quoted previously: $D_0 = 1.8(2)$ eV [12] and $D_0 = 1.7(2)$ eV [13].

The cumulative plot of the number of resonances as a function of neutron energy is shown in Fig. 11. The observed deviations from a straight line may indicate an increasing number of missing levels but they may be an artifact of statistical fluctuations. Table II lists the number of observed resonances with $J = 1$ and 2 in various energy ranges and gives a spacing obtained from these resonances.

For each region, the average spacing of resonances with a spin J is calculated as

$$D_{0,J} = \frac{\Delta E}{[N(J) - 1]}, \tag{18}$$

where ΔE is the energy difference between the last and the first resonance in the energy range and $N(J)$ is the number of resonances with spin J. The uncertainties in $D_{0,J}$ are conventionally estimated as $\sqrt{0.53/N}$, which is based on the expected Wigner distribution of resonance energies; this is the value quoted in Table II. The average spacing of the s-wave resonances D_0 is then obtained as

$$1/D_0 = 1/D_{0,1} + 1/D_{0,2}, \tag{19}$$

and the relative error in D_0 is calculated using the error propagation formula,

$$\sigma_{D_0} = \sqrt{\sigma_{D_{0,1}}^2 D_{0,2}^4 + \sigma_{D_{0,2}}^2 D_{0,1}^4}/(D_{0,1} + D_{0,2})^2. \tag{20}$$

Considering the limited number of resonances, the average spacings obtained from the various intervals agree reasonably well, suggesting that the fraction of missing resonances is small. For each energy interval the ratio $D_{0,1}/D_{0,2}$ is also listed. The result agrees very well with the expected $2J + 1$ value of 1.67.

We have two comments concerning this standard approach. First, it is widely accepted that there are long-range correlations in the positions of neutron resonances, as predicted by the Gaussian orthogonal ensemble (GOE). These correlations will significantly reduce the uncertainty in the resonance spacing with respect to the values given in Table II. Second, as already mentioned, the PT fluctuations almost surely prevent observation of all resonances. In order to estimate the fraction of missing resonances, we used simulations which were previously mentioned. In contrast to the fraction of missing neutron strength, the number of missing levels is rather sensitive to the value of the threshold for observation. Our simulations indicate that due to PT fluctuations in Γ_n^0, there must be a few resonances not observed even at low neutron energies. Unfortunately, it is very difficult to determine the exact number of the missing resonances; different simulated sequences of resonances give different numbers of missing levels and the number of missed resonances also depends on the adopted detection threshold. Nevertheless, we estimate that it is very unlikely to miss more than 10, 15, 21, and 30 resonances for energies below 60, 100, 140, and 180 eV, respectively. The most probable number of missing resonances is approximately half of the given maximum values.

Taking into account this estimate of the fraction of missing resonances, we suggest that the resonance spacing is $D_0 = 1.62(15)$ eV. The quoted error is probably rather conservative.

VI. SUMMARY AND CONCLUSIONS

The cross section of ^{155}Gd(n,γ) reaction for neutron energies 1.36–185 eV was measured with the DANCE calorimeter at the Los Alamos Neutron Science Center using

the time-of-flight method. Many resonances were observed. The resonance spin determines the details of the γ-ray decay and, therefore, also the multiplicity distributions. A novel approach has been developed that uses elements of pattern recognition theory to determine the spins of the capture resonances based on the γ multiplicity distribution observed. This method has the advantages that there is no need for selecting prototype resonances, that the maximum amount of information is utilized, and that a confidence level is obtained for the correctness of the spin assignment. This new method was applied to ^{155}Gd for which the spins of nearly all of the s-wave resonances were determined. These spins agree with those obtained from earlier, different, methods that were also based on observed multiplicity distributions. These results establish that the new pattern recognition method is a valuable addition to methods of determining the quantum numbers of resonances studied with the DANCE calorimeter.

Experimental data corrected for expected unobserved resonances give the s-wave level density $D_0 = 1.62 \pm 0.15$ eV. The separate level densities for the spin $J = 1$ and 2 resonances are in agreement with the expected $2J+1$ dependence.

Analysis of the cross-section data with the SAMMYcode also allowed the determination of neutron widths and, in a few cases, also the total radiative widths. Analysis of these results yielded an s-wave strength function of $S_0 = 1.99 \pm 0.28 \times 10^{-4}$ and an average total radiative width of $\Gamma_\gamma = 120 \pm 3$ meV. These numbers are in good agreement with previous experimental results.

ACKNOWLEDGMENTS

This work was supported in part by the US Department of Energy Grants No. DE-FG52-09NA29460 and No. DE-FG02-97-ER41042 and was performed under the auspices of the US Department of Energy by the University of California, Lawrence Livermore National Laboratory and Los Alamos National Laboratory under Contract No. W-7405-ENG-48 and No. W-7405-ENG-36, respectively. This work has benefited from the use of the LANSCE accelerator facility, supported under DOE Contract No. DE-AC52-06NA25396. It was also supported by the research plans MSM 0021620859 and INGO LA08015 of the Ministry of Education of the Czech Republic.

[1] S. A. Sheets, U. Agvaanluvsan, J. A. Becker, F. Bečvář, T. A. Bredeweg, R. C. Haight, M. Krtička, M. Jandel, G. E. Mitchell, J. M. O'Donnell, W. E. Parker, R. Reifarth, R. S. Rundberg, E. I. Sharapov, I. Tomandl, J. L. Ullmann, D. J. Vieira, J. M. Wouters, J. B. Wilhelmy, and C. Y. Wu, Phys. Rev. C **76**, 064317 (2007).

[2] M. Heil, R. Reifarth, M. M. Fowler, R. C. Haight, F. Käppeler, R. S. Rundberg, E. H. Seabury, J. L. Ullmann, J. B. Wilhelmy, and K. Wisshak, Nucl. Instrum. Methods A **459**, 229 (2001).

[3] R. Reifarth, T. A. Bredeweg, A. Alpizar-Vicente, J. C. Browne, E.-I. Esch, U. Greife, R. C. Haight, R. Hatarik, A. Kronenberg, J. M. O'Donnell, R. S. Rundberg, J. L. Ullmann, D. J. Vieira, J. B. Wilhelmy, and J. M. Wouters, Nucl. Instrum. Methods A **531**, 530 (2004).

[4] M. Jandel, T. A. Bredeweg, A. Couture, M. M. Fowler, E. M. Bond, M. B. Chadwick, R. R. C. Clement, E.-I. Esch, J. M. O'Donnell, R. Reifarth, R. S. Rundberg, J. L. Ullmann, D. J. Vieira, J. B. Wilhelmy, J. M. Wouters, R. A. Macri, C.Y. Wu, and J. A. Becker, Nucl. Instrum. Methods B **261**, 1117 (2007).

[5] J. M. Wouters, A. A. Vicente, T. A. Bredeweg, E. Esch, R. C. Haight, R. Hatarik, J. M. O'Donnell, R. Reifarth, R. S. Rundberg, J. M. Schwantes, S. A. Sheets, J. L. Ullmann, D. J. Vieira, and J. B. Wilhelmy, IEEE Trans. Nucl. Sci. **53**, 880 (2006).

[6] M. Jandel, T. A. Bredeweg, E. M. Bond, M. B. Chadwick, R. R. Clement, A. Couture, J. M. O'Donnell, R. C. Haight, T. Kawano, R. Reifarth, R. S. Rundberg, J. L. Ullmann, D. J. Vieira, J. B. Wilhelmy, J. M. Wouters, U. Agvaanluvsan, W. E. Parker, C. Y. Wu, and J. A. Becker, Phys. Rev. C **78**, 034609 (2008).

[7] F. Bečvář, Nucl. Instrum. Methods A **417**, 434 (1998).

[8] P. E. Koehler, J. L. Ullmann, T. A. Bredeweg, J. M. O'Donnell, R. Reifarth, R. S. Rundberg, D. J. Vieira, and J. M. Wouters, Phys. Rev. C **76**, 025804 (2007).

[9] F. Bečvář, P. E. Koehler, M. Krtička, G. E. Mitchell, and J. L. Ullmann, Nucl. Instrum. Methods Phys. A **647**, 73 (2011).

[10] K. Fukunaga, *Introduction to Statistical Pattern Recognition*, 2nd ed. (Academic Press, San Diego, 1990).

[11] G. J. McLachlan and T. Krishnan, *The EM Algorithm and Extensions* (John Wiley & Sons, New York, 1997).

[12] S. F. Mughabghab, *Atlas of Neutron Resonances* (Elsevier, Amsterdam, 2006).

[13] G. Leinweber *et al.*, Nucl. Sci. Eng. **154**, 261 (2006).

[14] N. M. Larson, Tech. Rep. ORNL/TM-9179/R7; ENDF-364/R, ORNL (2007).

[15] R. Capote, M. Herman, P. Obložinský, P. G. Young, S. Goriely, T. Belgya, A. V. Ignatyuk, A. J. Koning, S. Hilaire, V. A. Plujko, M. Avrigeanu, O. Bersillon, M. B. Chadwick, T. Fukahori, Zhigang Ge, Y. Han, S. Kailas, J. Kopecky, V. M. Maslov, G. Reffo, M. Sin, E. Sh. Soukhovitskii, and P. Talou, Nucl. Data Sheets **110**, 3107 (2009), available at [http://www-nds.iaea.org/RIPL-3].